DAMAGE-TOLERANT AIRCRAFT DESIGN

H.P. van Leeuwen*

Actions to be taken by an aircraft designer to realise a damage-tolerant structure and to have it certified are listed. Relevant work of the NLR is described.

1 INTRODUCTION

Present-day Airworthiness Requirements call for a so-called damage-tolerant aircraft design. In contrast to the safe-life philosophy adhered to earlier, the fail-safe or damage-tolerance philosophy allows the existence of flaws already at the time of the first flight, or developing later on in the life of the aircraft, due to fatigue, corrosion or accidental damage. It has to be demonstrated by analysis and/or test that the structure can sustain an appreciable load (of the order of limit load) in the presence of such a flaw, and that the flaw grows at such a low rate that it can be detected early enough to prevent a catastrophic failure.
The actions to be taken by an aircraft designer to realise a damage-tolerant structure and to have it certified have been presented by T. Swift (1) of the FAA and are listed in the left-hand column of the table below. The right-hand column lists relevant studies conducted at the NLR. The various actions required will be explained briefly and the NLR work will be reported on.

REQUIRED ACTIONS	RELEVANT STUDIES AT NLR
Define aircraft usage, missions.	Aircraft Integrated Data-System Records, usage analysis of B-747 aircraft operated by KLM, SAS and SWISS-AIR.
Develop load spectra, sequences.	AIDS Records, load monitoring RNLAF combat aircraft.
Select critical locations for an evaluation	
Develop stress spectra for those locations.	Development of test spectra TWIST (transport aircraft), FALSTAFF (fighters), HELIX/FELIX (helicopters).

*)National Aerospace Laboratory NLR, P.O. Box 90502, 1006 BM Amsterdam, The Netherlands

REQUIRED ACTIONS	RELEVANT STUDIES AT NLR
Determine environmental conditions for those locations.	
Compile crack growth data for each material and environment.	Crack growth studies on sheet, plate and forgings of several alloys.
Compile fracture toughness data.	Fracture toughness studies on above materials.
Produce crack growth curves.	Crack growth tests, computer program CORPUS for crack growth prediction, 3-D crack growth calculations for lugs.
Determine residual strength.	Residual strength test, computer programs ARREST (riveted structures), BOND (adhesive bonded structures).
Decide on inspection techniques.	Non Destructive Inspection, statistics of reliability, sensitivity and accuracy.
Determine detectable crack length.	Ditto.
Decide on inspection intervals.	Re-evaluation of design life of RNLAF combat aircraft.
ALTERNATIVE: Conduct full-scale test.	Full-scale test on wing of Fokker F-28 Fellowship.

2 AIRCRAFT USAGE

At the very beginning the designer has to decide what tasks the aircraft will have to perform. Will it be a civil or military transport, or will it be a combat aircraft? This will of course have a major effect on the design configuration and on the loads to be encountered in service. In the case of a civil transport it will make quite some difference whether the aircraft is designed for the transatlantic route, where at the usual high altitudes relatively little turbulence is experienced, or whether it will be operating on short-haul routes mainly overland. Similar considerations apply to military aircraft where one may distinguish e.g. long-range bombers, air defense or ground support combat aircraft. While for a transport loads will be mainly due to atmospheric turbulence (gusts), and manoeuvre loads will be relatively unimportant, the reverse applies to a combat aircraft. Relevant information is obtained through measurement or monitoring of usage and loading of aircraft already in service.
The NLR is engaged in such activities for both civil and military aircraft. Programs like the ones to be described are undertaken with a trifold aim:
- the provision of design data for future aircraft;
- the provision of loads data for use in realistic testing of materials, components or full-scale structures;
- the comparison of actual usage of the aircraft to the design usage, with the aim to adjust life estimates and inspection periods.

3 USAGE MONITORING OF B-747 AIRCRAFT

B-747 aircraft operated by KLM, SWISSAIR and SAS, who collaborate with UTA in the KSSU group, are equipped with an Aircraft Integrated Data System (AIDS). Under joint sponsorship by the Netherlands Civil Aviation Authoroty and KLM Royal Dutch airlines, NLR has developed and is operating a program whereby data on usage and loading of a sample of the aircraft involved are extracted from the AIDS records, processed and analysed, and stored for

later use. The program is described in, De Jonge and Spiekhout (2) and Spiekhout and Van Lummel (3), and illustrated in figure 1.
The AIDS system installed performs a continuous scanning of about 350 parameters. The data concern the flight as such, e.g. flight number, date, route, take-off weight. Furthermore they concern speed, Mach number, altitude, flap setting etc., and finally data directly related to the loading environment, such as vertical acceleration, cabin pressure and instantaneous weight.
The AIDS cassettes from the aircraft are processed on a routine basis in the computer facility of the operator by means of a number of application programs. The NLR-conceived B-747 FATIGUE program is one of these. The data extracted are stored on a magnetic tape which is sent to NLR for further processing. The AIDSREG program performs an extensive data quality check. As a result a flight may be totally or partly rejected. In the latter case a flag is added to the data indicating the particular error.
In August 1983 a total of 16222 flights covering about 80700 flight hours had been stored in AIDS FATIGUE DATA BASE.
The data are analysed by means of the ANALY program consisting of a usage statistics part and a load statistics part. The former produces general flight data tables and flight profile data tables. The latter produces vertical acceleration data and gust environment data. One type of flight profile data is the time spent in certain altitude bands and the related values of average weight and speed. The loads data are analysed using a "peak between means" counting method to be discussed later. Cabin pressure differential values are analysed because of their importance for fatigue of the fuselage.
One typical finding of the program is that during SWISSAIR flights from Zürich to Geneva the load factor experience is about as severe as that during a transatlantic flight to New York.
It is anticipated that the results from the NLR AIDS FATIGUE DATA program will provide an important input to Boeing's Supplemental Structural Inspection Program as it is applied to KLM-operated B-747s.

4 LOAD MONITORING OF RNLAF-OPERATED COMBAT AIRCRAFT

Under contract with the Royal Netherlands Air Force, the NLR has conducted a load monitoring program for Lockheed F-104G aircraft, Van Dijk (4). A similar program for the Northrop NF-5A/B aircraft has been in operation for some years now, De Jonge (5). Only the latter will be described presently. Approximately 20 percent of the aircraft in each squadron are equipped with a counting accelerometer of the so-called Fatiguemeter type. The instrument counts the number of times that a series of predetermined centre of gravity acceleration levels are exceeded. In addition, the number of manoeuvring flap actions is counted. Counting results are read out after each flight and entered in a debriefing form, together with information about mission type, flight duration, store configuration etc., see fig. 2. Data obtained in this way provide adequate information about the average load factor experience, the mission mix and the mission load factor spectra. Changes in utilization, leading to changes in load experience, are easily observed.
In addition, an operational NF-5A aircraft was equipped with relatively simple multi-parameter recording instrumentation (fig. 3).
The following quantities were measured:
- c.g. acceleration;
- strain gauge signal from centre wing bottom skin near rear spar;
- output strain gauge on manoeuvring flap actuator;
- speed;
- altitude;
- manoeuvring flap setting.

Acceleration and strains were scanned 12 times per second, the other quantities once per second. Scanned values were digitized and recorded on magnetic tape.
Typical results are presented in figure 4. As far as the loads are concerned, these are regularly presented to the RNLAF in the form of spectra such as illustrated in figure 6. Note the profound difference between the spectra for transport aircraft in figure 5 and the spectra for combat aircraft in figure 6. In order to arrive at spectra the raw loads data are processed, which means that they are compressed, filtered and counted. Now counting in this context is much more complicated than it sounds. In the present case the counting method used was the "restricted level crossings" or "fatigue meter count". This will be discussed later on.
The data obtained serve to advise the RNLAF on how fast the aircraft are using up their design life. This is facilitated by presenting the data also in the form of a "Load Severity Index". This LSI results from a relative Miner type analysis of the newly obtained data and the data compiled in 1974. In addition the data have been used to re-assess the service life by means of comparative fatigue tests on a representative wing skin specimen. This will be discussed in a later section.

5 COUNTING METHODS

As explained in Schijve (6), the aim of counting methods is to obtain a statistical distribution of characteristic magnitudes of load-time histories. An exhaustive summary is presented in table 1, taken from Van Dijk (7). A full description of all the methods mentioned is outside the scope of the present paper. Only those applied regularly by the NLR will be discussed.
As a first step a range filter is applied to delete small unimportant ranges, ripples superimposed on the major load excursions, from the record. This results in records such as shown in figure 4.
The PEAK BETWEEN MEANS counting method is rather straightforward. Its aim is to ignore small load variations, not crossing the mean load level, which are thought to be unimportant. This method is usually applied to VGH recordings and therefore it was selected for application to the B-747 AIDS FATIGUE DATA. The RESTRICTED LEVEL CROSSING counting method (Fig. 7) is more sophisticated. A level crossing in upward (downward) direction (e.g. level 2) is counted only after the load record has crossed a related level (e.g. 2') in a downward (upward) direction. The aim is to ignore level crossings from smaller load variations. The well known Fatiguemeter works according to this principle. Since the counting accelerometers used in RNLAF combat aircraft are of the Fatiguemeter type, this counting method was applied to the records discussed in section 4. As shown in figure 7, this method may suffer from some ambiguity.
More recently a more reliable counting method was developed independently at the NLR and by Japanese research workers. This is the RANGE PAIR RANGE count method or RAIN FLOW count method depicted in figure 8 and described in great detail in De Jonge (8). Counting is carried out in two phases. In the first phase all load cycles (range pairs) of an intermediate type are traced and counted in association with their respective mean values. After having been counted these intermediate cycles are successively deleted from the record. Finally the major load ranges remaining are counted, also in association with their mean values. This method most nearly represents the common view that fatigue damage is caused by load cycles and not by mere level crossings, peaks or unassociated positive and negative ranges.
This counting method is used by NLR for ad hoc studies, e.g. on the fin of the NF-5. The method is incorporated in a piece of apparatus called the

Spectrapot. This Swiss instrument is based on a microprocessor and provides on-board data reduction of a signal from e.g. a strain gauge applied at a critical location.

6 DEVELOPMENT OF TEST SPECTRA

The NLR has actively participated in the development of test spectra.
TWIST, the Transport Wing Standard, was developed together with the Laboratorium für Betriebsfestigkeit in Darmstadt.
FALSTAFF, the Fighter Aircraft Loading Standard for Fatigue evaluation, was developed together with, apart from LBF, the Industrie-Anlagen Betriebs-Gesellschaft and the Flugwerke Emmen.
HELIX/FELIX, load standards for helicopter rotors with hinged or fixed blades, were developed together with LBF, IABG, the Royal Aircraft Establishment and Messerschmitt-Bölkow-Blohm.
Presently work is going on for TURBISTAN, a load standard for turbine engine discs. In this program the three major European engine manufacturers participate, in addition to research institutes in France, Germany, the U.K. and Holland, and the University of Toronto.
TWIST and FALSTAFF are already used all over the world in national and in international programs of fatigue testing.
TWIST (De Jonge et al (9)) is based on measured and calculated load spectra for nine commercial transport (Fig. 5). The smooth average spectrum was approximated by a stepped function as is shown in figure 9. TWIST consists of blocks of 4000 different flights. There are ten different flight types, ranging from very rough (type A) to very smooth (type J). As shown in figure 9, there are also ten gust levels. All in all the TWIST sequence contains 398665 gust load cycles plus 4000 ground-air-ground cycles. Figure 10 shows part of a particular flight. Often the spectrum is truncated, i.e. load level I is reduced to equal II or III to avoid overly beneficial effects of high loads on fatigue crack propagation rate. Sometimes part of the lowest load cycles are omitted to speed up testing ("MINITWIST").
FALSTAFF (Van Dijk and De Jonge (10), De Jonge (11)) is based on measured flight load-time histories pertaining to five different fighter aircraft types operated by three different Air Forces. The spectrum as shown in figure 11 differs strongly from TWIST in that it is non-symmetrical and convex. Figure 12 shows a particular flight contained in the block of 200 different flights. These are a mix of three different mission types with three different manoeuvring severities. The complete sequence contains 35966 load levels of 32 different magnitudes. Zero stress level corresponds to FALSTAFF level 7.5269. Taxi load cycles are associated with zero stress level crossings.
HELIX and FELIX (Ten Have (12)) are based on measured loads for the Sea King and the Sikorsky CH-53 representing the hinged rotors, and on measured loads for the Bölkow BO-105 representing the fixed rotors. Calculated data for the Westland Lynx were used for comparison in the latter case. The loadings contained in the sequence are grouped according to four types of sorties with three flight lengths per sortie. The spectrum is based on a predetermined sequence of sorties, a predetermined sequence of manouevres within each sortie and a fixed load cycle sequence within each manoeuvre. Figures 13 and 14 give examples.
With TWIST and FALSTAFF the load sequence is derived from the spectrum using a random draw technique. With HELIX and FELIX the spectrum results from the sequence by application of a counting method (Figs. 15 and 16). The loadings within one manoeuvre, however, were determined by applying the rainflow counting method to actual flight records. The results were grouped together in so-called mean-stress/alternating-stress matrices, from which the load sequence was derived using a random draw technique.

7 IDENTIFICATION OF CRITICAL PARTS AND THEIR ENVIRONMENTS

The possibility to apply the damage tolerance philosophy depends on the structural materials involved.
If a material has a low fracture toughness, this means that cracks may grow in an unstable fashion, leading to catastrophic failure, before the crack has attained a size sufficiently large to allow detection by state of the art techniques. In this case the component cannot be considered damage tolerant. A safe life will have to be established on the basis of empirically determined lives to first crack and the appropriate safety factors. High-strength landing gear steels still fall in this category. If a material has a poor resistance to crack growth, the number of cycles or flights causing a crack to grow from the minimum detectable size to the catastrophic or critical size may be too small to accomodate a sufficient number (two or three) inspections. Present day engine disc materials are beginning to fulfill the requirement that cracks become critical at a length where they can be detected through non-destructive inspection, but this is mainly due to recent improvements in inspection techniques. Their fatigue crack growth resistance is stil being studied. This involves growth studies of very small cracks, which poses several problems. When considering damage tolerant structures one can distinguish between single load path and multiple load path structures, and also between inspectable and non-inspectable structures. The size of the initial flaw to be assumed in analysis may depend on it, see figure 17 taken from De Jonge (13). In the case of multiple load path structures secondary members will take on the load shed by the failing primary member. It is with such structures that the term "fail safe" originated. This classification has to be applied with caution since there may be a real chance that the secondary member has also developed a flaw. This is particularly germane to aircraft reaching or surpassing their design life. The penalty for having a non-inspectable structure is that its design life must be less than half or a third of the number of flights needed to propagate a crack to its critical size. Apart from damage tolerance the expression "durability" is now being heard. This is defined as the ability to resist cracking, corrosion, thermal degradation, delamination (composites!), wear and foreign object damage (Landy and Smithers (14)).
It is with such and other considerations in mind that the structural design is scanned for critical items. Figure 18 gives the flow diagram for the identification of critical parts that require special treatment by analysis and/or testing. This figure was taken from a booklet prepared within the framework of a program involving NLR employees acting as consultants to AERITALIA with respect to damage tolerance of their G-222 transport.
For the critical items identified also the service environment will have to be determined. It is well known that certain media may strongly accelerate crack propagation.
Possible environments can include:
- atmospheric condensate (contaminated by e.g. chlorides and sulphates);
- sump tank water;
- salt spray;
- de-icing fluids;
- exhaust gas.

Condensate usually forms when an aircraft descends from a high altitude where the temperature is low to a lower altitude where the temperature is higher and humidity is high. Structural elements in the vicinity of galleys and toilets are known to be subject to much corrosion. Salt spray or salt fog occurs at airfields near to the sea shore and most dramatically on aircraft carriers. De-icing fluids applied to the aircraft itself or to runways can be quite aggressive to some materials. Exhaust gases emanating from engines but also from weaponry can be quite aggressive too.

Proof of damage tolerance may be given on the basis of detailed analysis of flaw growth in the critical item. For that purpose load or load-factor spectra will have to be translated to stress spectra. Stress-per-g factors or stress-per-unit-load factors can be determined both by analysis and by testing.
Basic flaw growth data for material and environment are to be obtained by testing.

8 CRACK PROPAGATION TESTS

Fatigue crack growth in light alloys as sheet, plate and forgings is studied intensively at the NLR. In the last decade test results have been published at an average rate of four reports per annum. It would go too far to discuss all these results or even to list the reports. Instead some typical results will be presented.
Fatigue crack growth is studied for several purposes, e.g.:
- alloy evaluation;
- development of heat treatments;
- study of mechanisms;
- development of analytical models.

Figure 19 shows a forging that was designed especially to determine a set of characteristic engineering properties. Centre-notch flat specimens for fatigue testing are taken from the centre rib. Figure 20 gives a list of experimental heat treatments studied for the British AlZnMg alloy DTD 5024, (Van Leeuwen (15)). The heat treatments are compared on the basis of load cycles to propagate a crack from 2 mm halflength to 25 mm halflength, using a block type variation of load amplitude. Equipment for flight simulation testing was not yet available at the NLR. Figure 21 shows how this crack growth life correlates with tensile strength.
Results compiled by Schra (16) give crack propagation growth rates for four AlZnMg forging alloys tested under TWIST and FALSTAFF respectively. Ranking of the alloys was found to depend on the load spectrum applied. This means that material selection would be different for transport and for combat aircraft.
This is quite evident from figures 23 and 24, where the high-purity AlZnMg alloy 7475 is compared to the widely used AlCuMg alloy 2024 in sheet form. Note that crack growth acceleration and retardation due to high load amplitudes is much more pronounced for the weaker and tougher alloy 2024. These data were taken from Wanhill (17) and (18).
Figure 25 taken from Schijve et al (19) shows environmental effects on fatigue crack growth for the widely used sheet alloys 2024-T3 and 7075-T6. Note that crack growth rates are higher and environmental effects are more pronounced for the stronger alloy 7075 when tested under a gust load spectrum. Figure 26 taken from Wanhill (17) gives some more environmental effects for the alloys 2024 and 7075. Water spray was used to simulate condensate forming on descent from the cruise altitude. Salt water was sprayed with the aid of paint spray nozzles for a duration of two seconds halfway through each simulated flight.
Van der Linden (20) describes the development of a data base of fatigue crack propagation results to be used for the checking of predictive models of crack propagation. Basically a gust load spectrum derived for the Fokker F-27 Frienship was used. It was varied in a systematic way for more discriminative checking. This invloved three different gust load intensities (frequencies) and three ground-air-ground- cycle severities, giving nine conditions in all. The material was 2024-T3 Alclad sheet. Figure 32 shows a comparison of measured crack growth curves with those predicted with the

aid of a computerized model called CORPUS, to be described later (Van der Linden et al (21)).

9 RESIDUAL STRENGTH TESTS

At the NLR precracked specimens of light alloy sheet, plate and forgings are tested to determine residual strength or fracture toughness. The purposes of these tests are the same as listed for the fatigue crack propagation tests in section 8. A few examples will be presented.
Figure 22 shows some more results of the heat treatment studies of the AlZnMg alloy DTD 5024 (Van Leeuwen (15)). It is seen that heat treatments involving a cold quench as a rule lead to relatively high tensile strength but low fracture toughness.
Fracture toughnesses of four forged alloys were reported in (Schra (16)). Three specimen types were applied: Compact Tension, Single Edge Notch Bend and Centre Crack Tension. Since as usual the ASTM requirements for valid K_{IC} testing were not completely fulfilled "candidate fracture toughnesses" K_Q are presented in the first two cases. The high ductility demonstrated in the tests on CCT specimens forced us to present the "effective fracture toughness" K_e according to Feddersen.

$$K_e = \sigma_c(\pi a_o)^{0.5}. \qquad (1)$$

Here σ_c is the gross section stress at instability and a_o is the initial crack halflength. In addition the stress intensity factor at "pop-in" K_p was presented. K_p refers to a small arrested crack growth increment at relatively low load. Figure 27 shows residual strength values of 2 mm thick sheets of the aluminium alloys 2024-T3 and 7075-T6 (Vlieger (22)). Shown are straight lines depicting failure at general yield and also the failure curve according to Feddersen, consisting of a curve described by

$$K_c = \sigma_c(\pi a_c)^{0.5} \qquad (2)$$

and tangents to the points $\sigma = \sigma_y$ and $2a_c = w$. Here a_c is the crack halflength at instability. K_c is a useful measure of the fracture toughness if $\sigma_c \leq \frac{2}{3}\sigma_y$ and $2a_c \leq \frac{1}{3}w$, i.e. if the data points fall on the curve between the two points of tangency. Note that the ductile alloy 2024-T3 failed roughly at general yield.
Residual strengths are determined also for riveted and bonded stiffened panels. This is done in support of and for the checking of models to predict residual strength of built-up structures. Figure 29 (Vlieger (23)) shows some early configurations tested. Saw cuts are made in the panel centre, these may or may not be sharpened by fatigue. The centre stiffener may be present and intact, absent or present and cut. Upon loading the crack may first grow in a stable manner to be slowed down or arrested when approaching an adjacent stiffener. Failure may be initiated by stiffener rupture or unstable crack growth in the sheet. Crack growth is filmed and in later tests also measured with the electric potential drop method.
Figure 30 (Vlieger (22)) gives examples. The top picture shows no crack growth upon initial load increase, then some stable crack growth at further load increase and final failure due to stiffener rupture. The bottom picture also shows some stable crack growth, but then an increment of unstable crack growth (horizontal branch), crack arrest in a rivet hole and final failure due to stiffener rupture.

10 PREDICTION OF FATIGUE CRACK PROPAGATION

At the NLR fatigue crack growth models were developed for two configurations, i.e. a through crack in sheet material and a corner crack in a lug. The first model, called CORPUS, copes with interaction effects occurring under variable amplitude loading. The second so far does not have this capability. Van der Linden et al (21) describe the models in some detail. CORPUS is based on an empirical equation or law proposed by Paris already in the sixties.

$$\frac{da}{dn} = C(\Delta K)^m. \qquad (3)$$

Here da/dn is the crack growth per cycle and ΔK is the range of the stress intensity factor associated with that cycle. C and m are empirical constants. Now K is the stress intensity factor which can be written as:

$$K = S.\sqrt{\pi a}.f(\frac{a}{w}) \qquad (4)$$

where S is the nominal gross section stress, a is the crack (half)length and w is the (semi)width. The function f(a/w) copes with variations in geometry. It has been documented accurately for a series of standard configurations. It follows that:

$$\Delta K = \Delta S.\sqrt{\pi a}.f(\frac{a}{w}). \qquad (5)$$

The problem with variable amplitude loading is that ΔS will not simply equal the nominal stress range but has to equal the effective stress range ΔS_{eff}. This is because plasticity at the crack tip or plasticity in the wake of the crack will cause the crack not to close at zero stress or to close and to open at a stress different from zero, i.e. S_{op}. Now

$$S_{eff} = S_{max} - S_{op} \qquad (6)$$

and the trick is to predict S_{op}, which will depend not only on the last stress range applied, but also on some stress ranges applied previously. This is because a high stress applied at some cycle may cause a large plastic deformation at the crack tip, which may show up as a hump on the crack surface or contour during later cycles when the crack tip has proceeded further. S_{op} is the stress at which the highest humps near the crack tip lose contact upon load increase. A complicating factor is that a hump may be flattened (reduced in height) upon application of some minimum stress S_{min}. The model pressumes that a hump has an effect only as long as the crack tip is inside the primary plastic zone that was formed when the hump was formed. Figure 31 depicts some successive steps in crack growth and development of opening stresses S_{op}. Diagram (a) shows a succession of nominal stress cycles. (b) again shows the first cycle. (c) shows how S^1_{op} is obtained from an empirical relation between S_{op}/S_{max} and the stress ratio $R = S_{min}/S_{max}$. Note that in more recent versions of the model S_{op} is calculated directly using the strip yield model of Dugdale and Barenblatt. (d) shows how S^1_{op} is related to the first stress range, and (e) shows how the crack does really open at S^1_{op} during the second cycle. Further diagrams show development of further crack opening stresses S^2_{op} and S^3_{op}, and their decrease due to low stresses S^2_{min} and S^3_{min}, with a lowered S^1_{op} remaining the governing opening stress until the fourth cycle, with S^4_{op} exceeding S^1_{op} and becoming the governing one. Figure 32 shows how well CORPUS predicts crack growth determined empirically. The model also accounts for the effect

on plastic zone size of a plane-strain to plane-stress transition as the crack grows relative to the sheet thickness.
The second model is depicted in figure 33. It essentially computes stress intensity factors at the crack front and along trajectories orthogonal to the crack fronts. Crack propagation is again predicted as a function of the stress intensity range using Paris' law. Stress intensity factors are calculated by finite element analysis using the ASKA system. The K-factors are deduced from the energy release rate calculated through the virtual crack extension and stiffness reduction method. Since this is rather cumbersome an approximation is made for many steps involving an extrapolation of K-values for growing crack size using estimated gradients dK/da. The accuracy of the approximation is checked at intervals. The accuracy of the model as such was verified by comparison of the predictions with fatigue test results. In these tests marker loads were applied to determine the crack front shape. For some calculations K-values are estimated from data banks for given shapes (quarter ellipses) rather than by FEM analysis. It is found that although stress intensities may vary strongly along the crack front, the latter develops in a rather stable manner, and K-values tend to converge. Care is taken to stay away from the free surfaces in order to avoid having to deal with plane stress effects.

11 PREDICTION OF RESIDUAL STRENGTH OF CRACKED STIFFENED PANELS

At the NLR two computer programs were developed to predict the residual strength of flawed built-up structures. ARREST predicts the behaviour of cracked riveted panels and BOND does the same for cracked adhesive bonded panels. The principles of the methods are described in Vlieger (24) and (25). The programs are described in detail in Vlieger and Sanderse (26) and Vlieger (27).
The principles are explained in figure 34. In both diagrams there are given three dashed curves for the residual strength of the unstiffened sheet. These are essentially Feddersen type curves as already shown in figures 27 and 28. The bottom line gives the stresses at the onset of stable crack growth, the top one gives the stresses at the onset of crack instability, and the middle one relates the residual strength σ_c to the initial crack length. In the case of a crack in a stiffened sheet, however, the residual strength can be higher because when a crack tip approaches a stiffener, the sheet will shed some of its load on that stiffener. In the calculations there is introduced a stress intensity reduction factor:

$$C(a) = \frac{K_{stiffened}}{K_{unstiffened}} \leq 1 \qquad (7)$$

Hence for the stiffened sheet there results:

$$K_{stiffened} = C(a)\sigma\sqrt{\pi a} \qquad (8)$$

and the allowable panel end-stress σ_{sh} based on sheet failure becomes

$$\sigma_{sh}(a) = \frac{K_c}{C(a)\sqrt{\pi a_c}} = \frac{\sigma_c}{C(a)} > \sigma_c \qquad (9)$$

As a consequence the load on the stiffener is increased locally. This gives rise to a stiffener load concentration factor:

$$L(a) = \frac{F_{max}}{F_{remote}} \geq 1 \qquad (10)$$

Stiffener failure will occur if the local stiffener stress reaches the ultimate strength σ_{ult}, i.e.

$$L(a).\sigma.A_{st} = \sigma_{ult}\,A_{st} \qquad (11)$$

where A_{st} is the stiffener cross sectional area.
Hence the allowable panel end-stress σ_{st} based on stiffener failure becomes

$$\sigma_{st}(a) = \frac{\sigma_{ult}}{L(a)} < \sigma_{ult}. \qquad (12)$$

In figure 34 a/b it is shown how $\sigma_{st}(a)$ decreases with increasing crack length and how $\sigma_{sh}(a)$ rises above $\sigma_c(a)$ as the crack grows. Three modes are depicted. Note that in the top figure σ_{sh} rises above σ_{st} whereas in the bottom figure this is not the case.
For a short crack $2a_1$ in figure 34a we see how upon load increase there is first some stable crack growth, then unstable crack growth and immediate stiffener failure without further load increase. For a long crack $2a_2$ there is again stable and unstable crack growth but the crack arrests as the σ_{sh} curve is reached for the second time. Some small load increase is again possible but soon leads to stiffener failure and final fracture. In the bottom figure both for short and for long cracks there is crack arrest, the load can increase but not beyond $\sigma_{sh,max}$. This leads to a second burst of unstable crack growth, stiffener failure and final fracture. It should be noted that the two models can cope with plasticity effects for sheet, stiffeners, fasteners and adhesive.
The models are already able to predict fatigue crack growth, since they produce values of the stress intensity factor as the crack grows. Stiffener failure due to fatigue can be predicted also because a Miner type analysis can be executed on the rising stiffener load level values. Work is now going on incorporating the fatigue crack growth model CORPUS for variable amplitude loading.

12 NON-DESTRUCTIVE INSPECTION

In order to apply damage-tolerance principles in design and operation of aircraft one has to be able not only to predict crack growth, but also to detect flaws and to measure their size, should they really arise in service. Studies of the reliability of inspection methods are necessary because they give the data upon which one has to base:
- selection of inspection techniques;
- determination of minimum detectable flaw sizes;
- prescription of inspection periods.

At the NLR statictical studies into the reliability of inspection methods were made involving two batches of specimens. These studies are described in De Graaf and De Rijk (28) and De Graaf (29).
The first batch consisted of 102 plate specimens made of two AlCuMg type aluminium alloys. They have been provided with a milled recess imitating the rabbet of an inspection porthole in a wing skin. The specimens were fatigued in three-point bending to produce cracks in the fillets. Inspection techniques used comprised eddy current, ultrasonics and penetrant. In the first two cases the inspections were conducted from the flat outer surface. The first inspection results were recorded. It was noted that with eddy current 159 cracks out of 198 were detected, with ultrasonics 123 out of 198 and with penetrant 188 out of 194.

After the first inspection the specimens were corroded for three weeks in a salt fog chamber. Subsequently they were inspected for a second time. Finally the specimens were broken to reveal the actual crack sizes. It was noted that eddy current and ultrasonics tended to underestimate the crack lengths strongly. The data were analysed statistically to determine the reliability of the inspections used. The reliability is the percentage of the detected defects of a particular size as a function of that size. The results are presented in figure 35 as the probability of detection $\bar{p}$ and its lower limit p_l with 95 % confidence. It is seen that corrosion strongly affects the reliability of the techniques. The results indicate superiority of penetrant inspection before corrosion but superiority of eddy current inspection after corrosion. Selections of minimum detectable crack sizes can be based on these results. After this investigation the specimens could not be used in subsequent programs of course. This drawback was avoided with the second batch. This consisted of 201 low-alloy high-strength steel drag struts from a combat aircraft landing gear as sketched in figure 37. At one end these struts had protruding lugs used for locking the gear in the extended position. Fatigue cracks had been found to occur frequently in the fillets at one of the edges of these lugs. Part of the drag struts had been rejected because they had exceeded their safe life and others because of cracks found in periodic inspections. So there were three possible flaw sites per strut but cracks could be expected only at part of these sites. How many was not known precisely, since this depended on the inspections carried out. The estimate was updated after every inspection run. Only four struts were investigated destructively, so now there remain 197 for future investigations. These struts are offered to interested parties for checking the reliability of the techniques they use and for adding to the data base developed.
An unambiguous way of lug identification was adopted and the struts were inspected successively by a number of inspectors using ultrasonics, fluorescent penetrant, fluorescent magnetic ink, magnetic rubber and eddy currents. Each inspector applied as many techniques as possible. As was stated earlier the specimens but four were not tested destructively. Instead a lug was considered to be flawed if the majority of the inspections indicated this to be the case. In figure 37 the results are given in terms of percentage of missed flaws and percentage of flaws erroneously indicated as being present. Statistical analysis produced a probability of detection in the first case and a probability of recognition in the second case. In both cases the 95 % confidence level was adhered to.

13 RE-ASSESSMENT OF SERVICE LIFE

The initiation and propagation of fatigue cracks can be predicted using more or less sophisticated methods. They can still be studied empirically as well. For the results of such tests to be meaningfull for the real structure, the specimen as well as the load history should truly represent the service situation.
A specimen developed for representing the wing skin of the Northrop F-5A/B was described by De Jonge (5). During the full-scale testing of the aircraft by the manufacturer a cut-out in the rear edge of the bottom wing skin near the root rib was established as a critical location. At the NLR a specimen was designed for which the geometry and the stress distribution were identical to those in the wing skin. The local stress distribution in the wing was determined with the aid of resistance strain gauges. It was also calculated using a finite element method. The shape of the specimen had to be such that simple tensile loading would produce the same stress distribution as the complex loading of the skin in the wing structure. Finite elements were used in a trial and error approach. In order to be able to

perform the fatigue tests in a machine of limited capacity the specimen thickness was scaled down to half size. Care was taken, however, to use the same material and heat treatment as in the aircraft, the same grain direction, the same surface roughness and protective treatment, and even a rib flange was added, fastened to the skin in exactly the same way as in the aircraft. Finally the calculations were verified by strain gauge measurement.
As was discussed in section 4, information on the loadings actually encountered in service had been determined on a routine basis. From the data compiled in 1974 a representative load spectrum was constructed, indicated as BASIC-MOD. This was used in comparative fatigue tests on the specimen discussed above. In the ideal case this basis of comparison would have been the load spectrum as used in the full-scale test by the manufacturer, figure 36. This would have enabled a straightforward correction of life to first crack and crack propagation rate. Unfortunately this spectrum was not available. Instead comparative tests were done using a block-type load spectrum that had been used by Northrop on structural details. Tests have been done also using the FALSTAFF spectrum. Similar tests were done later on behalf of the Canadian Armed Forces using a loading pattern representative for Canadian usage of the CF-5 aircraft. In the latter case full-thickness specimens were tested in a large capacity fatigue machine. Tests have also been done to investigate the effects of surface treatments on fatigue life.
It is often found that the usage of an aircraft and its loading experience change from year to year. For an assessment of the effects of such changes calculations of a Load Severity Index as described in section 4 can be made. A newer approach involves the calculation of crack growth from a fictitious flaw under loading pattern measured in service. Such calculations should be checked occasionally by testing, especially if the loading pattern deviates strongly from that originally assumed or experienced.

14 FULL-SCALE FATIGUE TEST ON THE WING OF THE FOKKER F-28 FELLOWSHIP

A detailed damage-tolerance analysis involving calculations of crack growth and residual strength, supported by tests on materials and structural details is seen as an alternative to a full-scale fatigue and residual strength test. In many cases, however, these two approaches cannot fully replace one another. In such cases both approaches will often be followed to some extent. In the late sixties the NLR conducted the full-scale test on the wing structure of the Fokker F-28 Fellowship. An artist impression of the set-up, taken from Fonk (32), is presented as figure 38. Details are reported in De Jonge (31), (32) and Noback (33).
The wing was surrounded by a steel framework and was hanging from it on four struts attached to the fittings of the wing-to-fuselage joints. Movement in spanwise direction was prevented by beams attached to the brackets of the main-landing-gear-door actuators. Movement in flight direction was prevented by beams attached to the brackets of the landing gear side stays.
As can be seen in figure 38, six hydraulic jacks loaded the wing from above and another six loaded it from below. Not shown are the whiffle trees distributing the load in span- and chordwise direction. Mean load in flight and gust loads were applied by four jacks from above, i.e. near the wing tip and near the leading edge at mid-span. Their loads were distributed by whiffle trees. Attachment to the wing structure was by adhesive bonded pads to the skin and by strips riveted to the nose ribs. A constant downward correction load was applied by two jacks below the wing near the wing tips. During simulated landings and take-offs the remaining six cylinders came into play. Two jacks from above applied upward flap loads during the approach phase. Two cylinders below the wing near mid-span applied downward loads through wiffle trees. Another two cylinders nearer to the wing root applied upward landing gear loads.

Load control was of the closed-loop type involving five channels since, as indicated earlier, two cylinders had to apply a constant downward load only. The control equipment comprised a piece of apparatus called PAGE (Programmed Amplitude GEnerator). The program was fed in by punched tape, which was still state of the art then. The gust load program applied was akin to TWIST. There were 11 gust load levels and 10 different flights of different gust load severity. The highest load in the sequence had a probability of occurrence of once per 5000 flights. As compared to TWIST there were far less cycles per flight, however.
During the test inspections for cracks were carried out daily by NLR personnel. Major inspections by Fokker personnel were carried out once per 5000 flights. Fatigue testing for 60 000 flights resulted only in some minor nuisance cracking in the wing leading edge structure at the points of load application. In order to speed up testing, the lowest load level was omitted during the next 40 000 flights. After completion of 100 000 flights artificial cracks were sawed at 10 locations. In order to avoid beneficial effects from high loads the highest load level was omitted. After flight 110 000 the lowest load level was re-introduced since it was expected to contribute to crack growth. In the meantime 10 natural cracks had been detected. After 119 000 flights 7 natural cracks were repaired and 11 new artificial cracks were made. Another 10 natural cracks were found. The fatigue test was ended after slightly more than 147 000 flights. After repair of 7 cracks the fail sale load equal to limit load was applied three times. Between tests only 3 artificial cracks had been repaired. The wing fully qualified as a damage tolerant structure.

15 REFERENCES

1. Swift, T., Application of Damage Tolerance Technology to Type Certification. SAE Tech. Paper 811062. SAE Aerospace Congress & Exposition, Anaheim CA, 1981.

2. De Jonge, J.B. and Spiekhout, D.J., Use of AIDS Recorded Data for Assessing Service Load Experience. NLR MP 77011 U, 1977. Also ASTM STP 671, pp. 48-66.

3. Spiekhout, D.J. and Van Lummel, C.W.J., Operational Loads on B-747 Aircraft: Design Assumptions, Actual Experience and Maintenance Aspects. NLR MP 83051 U, 1983.

4. Van Dijk, G.M., Re-assessment of Fatigue Performance of Fighter Aircraft. NLR MP 73027 U, 1973. Also AGARD CP-141, pp. 7/1-7/19.

5. De Jonge, J.B., Re-assessment of Service Life by Comparative Specimen Tests. NLR MP 79008 U, 1979. Tenth ICAF Symposium Brussels, 1979.

6. Schijve, J., The Accumulation of Fatigue Damage in Aircraft Materials and Structures. AGARD CP No. 118, 1972, pp. 3/1-3/120.

7. Van Dijk, G.M, Statistical Load Data Processing. NLR MP 71007 U, 1971, Sixth ICAF Symposium Miami Beach.

8. De Jonge, J.B., The Analysis of Load Time Histories by Means of Counting Methods. NLR MP 82039 U, 1982, AGARD AG-292, Helicopter Fatigue Design Guide.

9. De Jonge, J.B., Schütz, D., Lowak, H. and Schijve, J., A Standardized Load Sequence for Flight Simulation Tests on Transport Aircraft Wing Structures. NLR TR 73029 U, 1973. Also LBF FB-106.

10. Van Dijk, G.M. and De Jonge, J.B., Introduction to a Fighter Aircraft Loading Standard for Fatigue Evaluation "FALSTAFF" (Part I). NLR MP 75017 U, 1975, Eight ICAF Symposium, Lausanne.

11. De Jonge, J.B., Additional Information about FALSTAFF. NLR TR 79056 U, 1979.

12. Ten Have A.A., HELIX and FELIX: Loading Standards for Use in Fatigue Evaluation of Helicopter Rotor Components. NLR MP 82041 U, 1982. AGARD AG-292 Helicopter Fatigue Design Guide.

13. De Jonge, J.B., The Requirement of Damage Tolerance. An Analysis of Damage Tolerance Requirements with Specific Reference to MIL-A-83444. NLR TR 77005 L, 1977.

14. Landy, M.A. and Smithers, O.L., Durability and Damage Tolerance Control Plans for USAF Aircraft. AIAA Paper 82-0678. AIAA/ASME/ASCE/AHS 23rd Structures, Structural Dynamics and Materials Conference, New Orleans LA, 1982.

15. Van Leeuwen, H.P., Optimum Heat Treatment of Al-Zn-Mg Alloys of the DTD 5024 Type. NLR MP 72035 U, 1972. Also Metallurgia and Metal Forming, Vol. 40, No. 12, p. 379, 1973.

16. Schra, L., Engineering Property Comparisions for Four AlZnMgCu Type Forging Alloys. NLR TR 79022 U, 1979.

17. Wanhill, R.J.H.., Flight Simulation Environmental Fatigue Crack Propagation in 2024-T3 and 7475-T761 Aluminium. NLR MP 80003 U, 1980.

18. Wanhill, R.J.H., Manoeuvre Spectrum Fatigue Crack Propagation in Aluminium Alloy Sheet Materials. NLR TR 78091 U, 1978.

19. Schijve, J., Jacobs, F.A. and Tromp, P.J., Environmental Effects on Crack Growth in Flight-Simulation Tests on 2024-T3 and 7075-T6 Material. NLR TR 76104 U, 1976.

20. Van der Linden, H.H., NLR Test Results as a Data Base to be Used in a Check of Crack Propagation Prediction Models, A GARTEUR Activity. NLR TR 79121 L, 1979.

21. Van der Linden, H.H., De Koning, A.U. and Lof, C.J., New Analytical Methods for the Prediction of Fatigue Crack Growth Under Realistic Loading. NLR MP 82055 U, 1982. International Journal of Vehicle Design, Special Issue, 1984.

22. Vlieger, H., Residual Strength Data of Riveted Panels with Different Stiffener Configurations. NLR TR 76033 U, 1976.

23. Vlieger, H., Residual Strength of Cracked Stiffened Panels, NLR TR 71004 U, 1971.

24. Vlieger, H., Fail-safe Characteristics of Built-up Sheet Structures. NLR MP 74017 U, 1974. Ninth Congress of ICAS, Haifa.

25. Vlieger, H., Application of Fracture Mechanics to Built-up Structures. NLR MP 79044 U. AGARD AG-257 Practical Applications of Fracture Mechanics.

26. Vlieger, H. and Sanderse, A., User's Manual of ARREST, a Computer Routine for Prediction of Residual Strength of Cracked Stiffened Panels. NLR TR 75129 C, 1975.

27. Vlieger, H., Residual Strength of Bonded Stiffened Panels: Prediction and Experimental Verification. NLR TR 83066 L, 1983.

28. De Graaf, E.A.B. and De Rijk, P., Comparison Between Reliability, Sensitivity and Accuracy of Non-Destructive Inspection Methods. NLR MP 81009 U, 1981. Thirteenth Symposium on Non-Destructive Evaluation, San Antonio, Texas.

29. De Graaf, E.A.B., Presentation of NDT-Reliability Curves. NLR TR 82076 L, 1982.

30. Fonk, G.J., Investigation of the Fail-Safe Properties of Civil Aircraft. Fokker Aircraft Company. Seventh ICAF Symposium, London, 1973.

31. De Jonge, J.B., General Description of the Fatigue Test on the Wing of the F-28 Fellowship (TA.07) NLR TR 68051 C, 1968.

32. De Jonge, J.B., F-28 Wing Fatigue Test. The Magnitude, Number and Sequence of the Gust Loads to be Applied in the Test. NLR TR 68065 C, 1968.

33. Noback, R., Description of the Equipment for the Fatigue Test on the Wing of the Fokker F-28 Fellowship. NLR TR 70008 L, 1970.

TABLE 1
COUNTING PROCEDURES

SIMPLE LEVEL-CROSSING COUNT METHOD RESTRICTED LEVEL-CROSSING METHOD
SIMPLE PEAK COUNT METHOD LEVEL-RESTRICTED PEAK COUNT METHOD RANGE-RESTRICTED PEAK COUNT METHOD PEAK-BETWEEN-MEAN-CROSSINGS COUNT METHOD
SIMPLE RANGE COUNT METHOD RANGE-MEAN COUNT METHOD RANGE-PAIR EXCEEDANCE COUNT METHOD RANGE-PAIR-RANGE COUNT METHOD

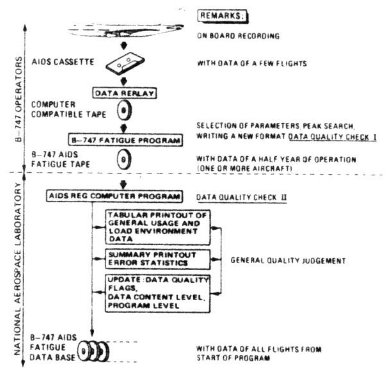

Fig. 1 Summary of B–747 AIDS–fatigue data acquisition

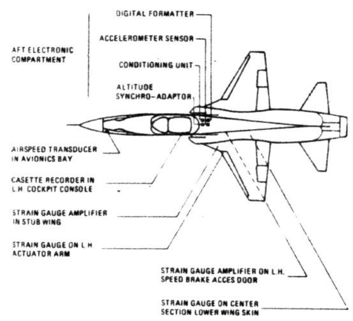

Fig. 3 Instrumentation used for multiparameter usage recording

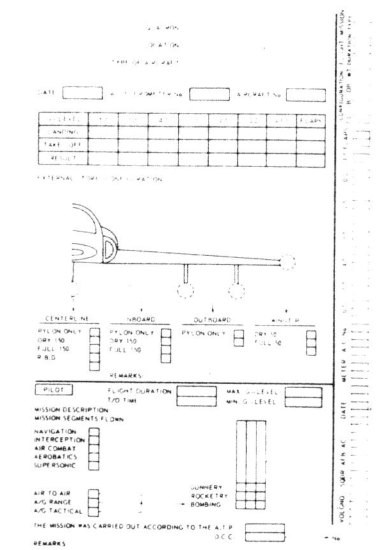

Fig. 2 Debriefing form used with counting accelerometers

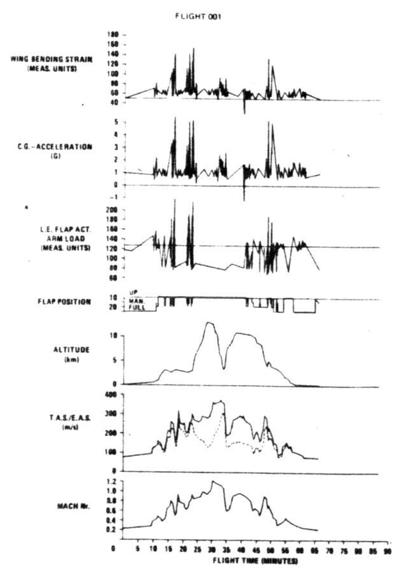

Fig. 4 Typical example of multiparameter flight–load history obtained

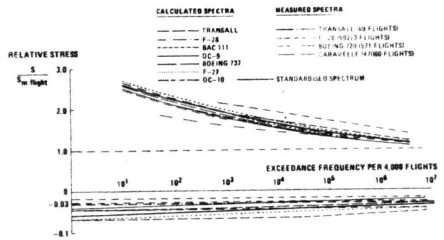

Fig. 5 Load spectra pertaining to 40,000 flights for different aircraft

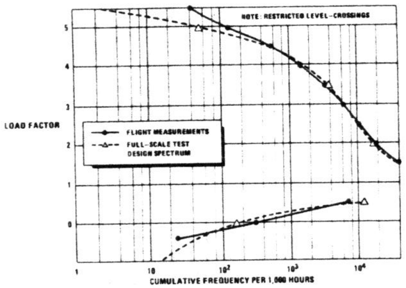

Fig. 6 Combat aircraft load spectra

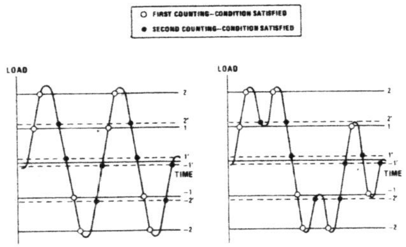

Fig. 7 Restricted level–crossing count method

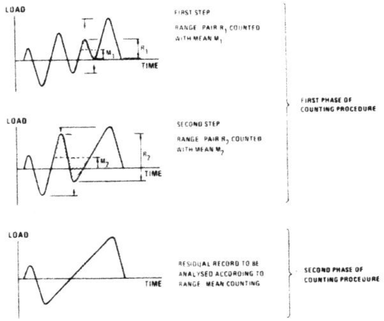

Fig. 8 Illustration of range–pair–range count method

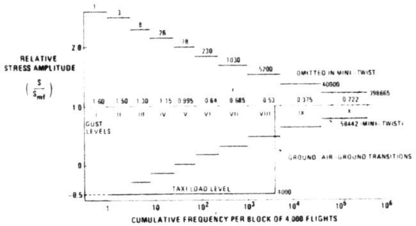

Fig. 9 The test load spectrum pertaining to TWIST and MINI–TWIST

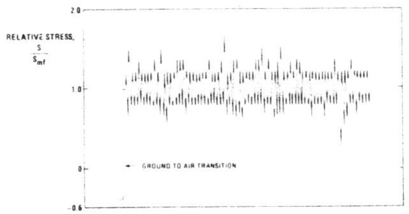

Fig. 10 Cutout of a "D"–flight loading trace within TWIST

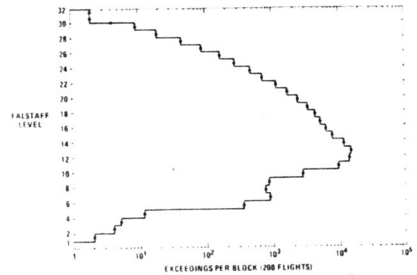

Fig. 11 FALSTAFF load spectrum

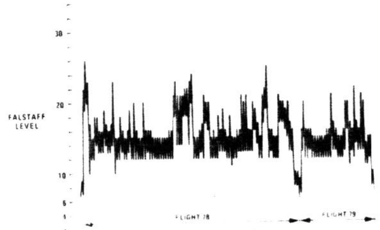

Fig. 12 Part of FALSTAFF sequence

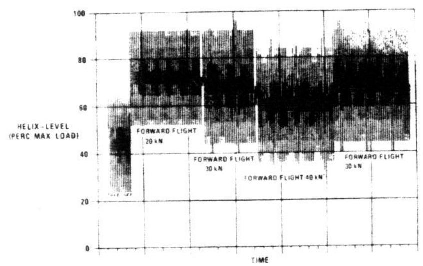

Fig. 13 Beginning of HELIX training–flight (representing 90 seconds flight time)

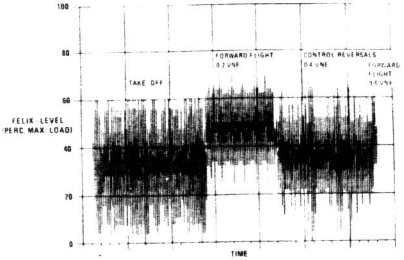

Fig. 14 Beginning of FELIX training–flight (representing 84 seconds flight time)

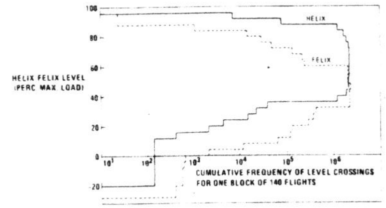

Fig. 15 HELIX/FELIX level cross counting

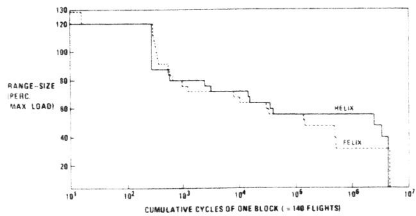

Fig. 16 Comparison of HELIX and FELIX overall spectra (full cycles, rainflow counting technique)

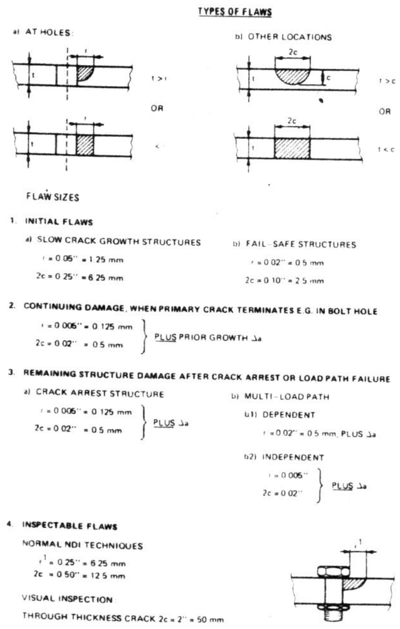

Fig. 17 Summary of flaw–assumptions

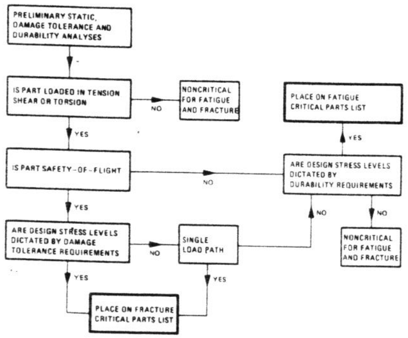

**Fig. 18 Identification of critical areas (I):
Selection of fatigue and fracture critical parts**

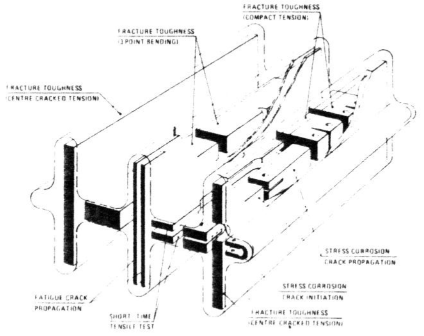

Fig. 19 The general appearance of a forging and the type and position of the test specimens used to evaluate engineering properties

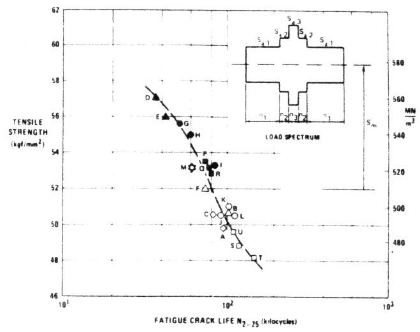

Fig. 21 The relationship between strength and fatigue cracking resistance for various heat treatments of the AlZnMg Alloy DTD 5024

SYMBOL AND NUMBER		SOLUTION HEAT TREATMENT	QUENCH BATH TEMP	PRIMARY AGEING	SECONDARY AGEING
◇	A	460°C 10 min	100°C	NONE	135°C 15 hours
◇	C	460°C 360 min	DITTO	NONE	DITTO
△	B 1)	460°C 90 min	100°C	NONE	135°C 15 hours
△	F	DITTO	DITTO	100°C 15 hours	DITTO
○	J	460°C 90 min	100°C	100°C 15 hours	150°C 15 hours
○	K	DITTO	DITTO	120°C 15 hours	DITTO
○	L 2)	DITTO	DITTO	135°C 15 hours	DITTO
□	U	460°C 90 min	100°C	100°C 15 hours	180°C 0.5 hour
□	T	DITTO	DITTO	DITTO	180°C 1 hour
□	S	DITTO	DITTO	DITTO	180°C 4 hours
▲	D	460°C 90 min	10°C	NONE	135°C 15 hours
▲	E	DITTO	DITTO	100°C 15 hours	DITTO
●	G	460°C 90 min	10°C	100°C 15 hours	150°C 15 hours
●	H	DITTO	DITTO	120°C 15 hours	DITTO
●	I	DITTO	DITTO	135°C 15 hours	DITTO
■	P	460°C 90 min	10°C	100°C 15 hours	180°C 0.5 hour
■	Q	DITTO	DITTO	DITTO	180°C 1 hour
■	R	DITTO	DITTO	DITTO	180°C 4 hours
✿	M		AS RECEIVED		

1) STANDARD TREATMENT DTD 5024
2) STANDARD TREATMENT DTD 5104

Fig. 20 Treatments applied to Alloy DTD 5024

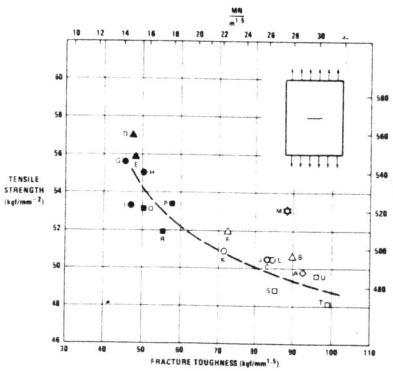

Fig. 22 The relationship between strength and fracture toughness for various heat treatments of the AlZnMg Alloy DTD 5024

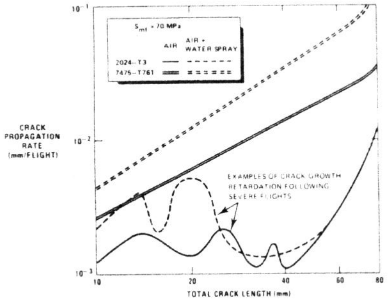

- 2024 RATES ACCELERATED BY AIR + WATER SPRAY ONLY AT SHORT CRACK LENGTHS
- 7475 RATES ACCELERATED BY AIR + WATER SPRAY AT ALL CRACK LENGTHS
- SEVERE FLIGHTS CAUSE LARGE AND PERSISTENT CRACK GROWTH RETARDATIONS FOR 2024

Fig. 23 Environmental effects on crack propagation rates for 2024 and 7475 with TWIST

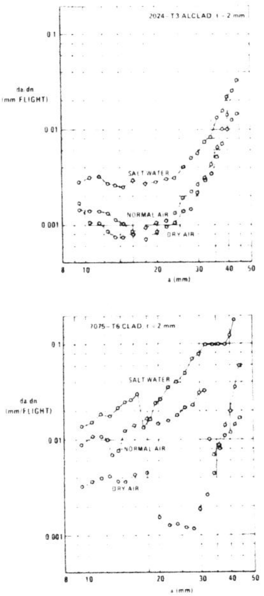

Fig. 25 Environmental crack propagation rate for S_{mf} = 70 MN/m^2 in 2 mm material

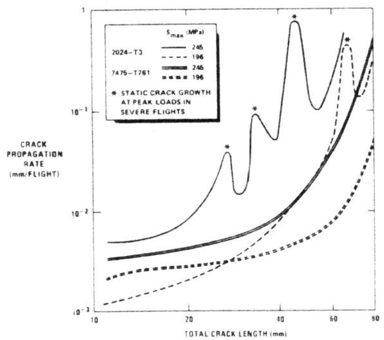

- HIGH STRESS LEVELS (S_{max} = 245 MPa) 2024 RATES ALWAYS FASTER AND STATIC CRACK GROWTH OCCURS AT SHORT CRACK LENGTHS
- LOW STRESS LEVELS (S_{max} = 196 MPa) 2024 RATES INITIALLY LESS THAN 7475 RATES

Fig. 24 Crack propagation rates for 2024 and 7475 with FALSTAFF

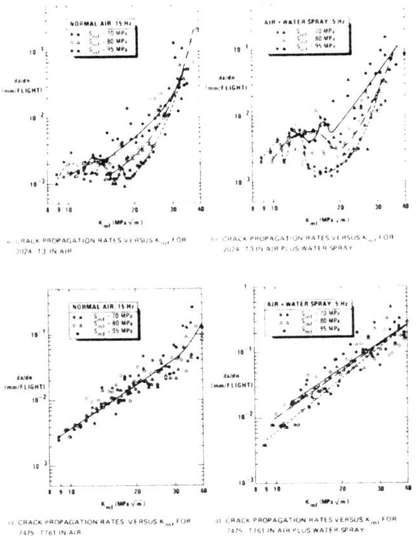

Fig. 26 Various crack propagation rate curves

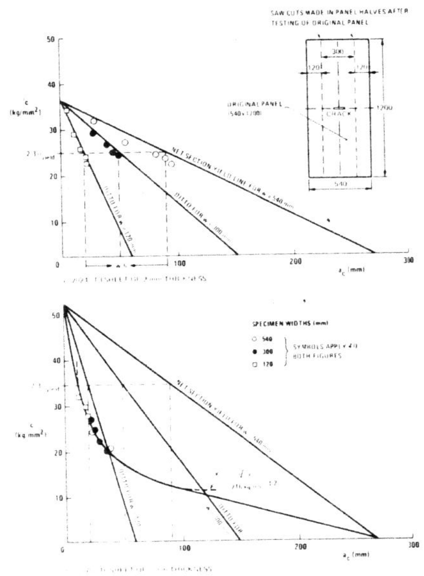

Fig. 27 Results of residual strength tests on unstiffened panels of different widths

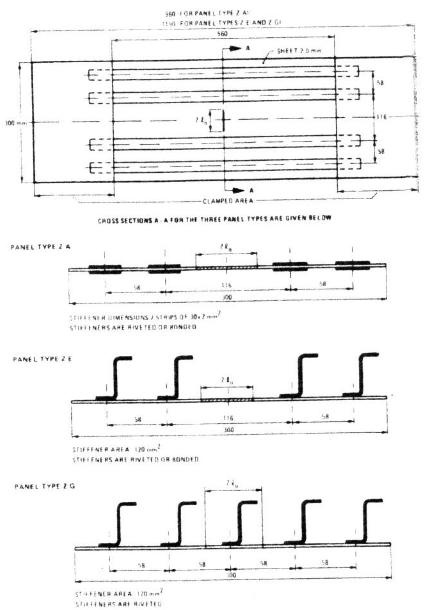

Fig. 29 Dimensions (mm) and detailed geometry of specimens

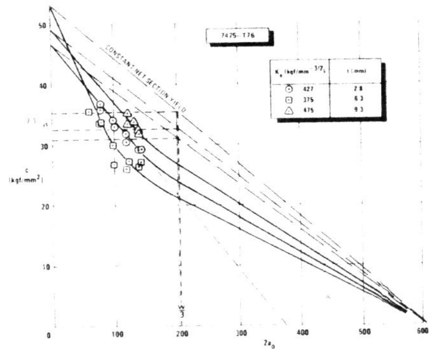

Fig. 28 Fracture stress as a function of initial crack size

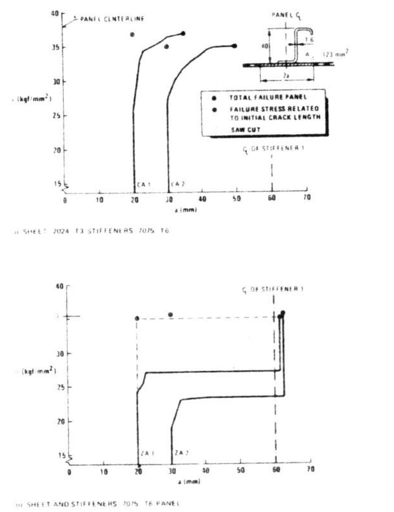

Fig. 30 Results of residual strength tests on panels with 9 Z–stiffeners and a central saw cut in the skin. Panel width: 540 mm. Stiffener spacing: 60 mm

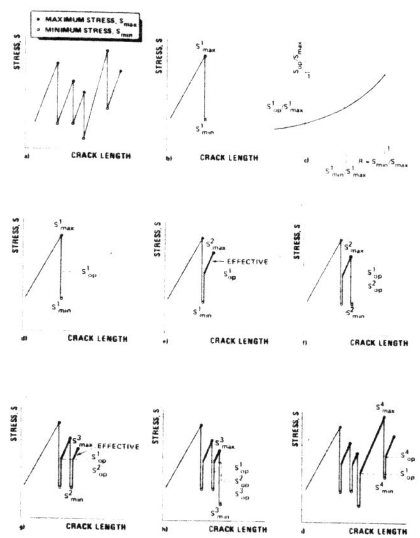

Fig. 31 Crack opening behaviour

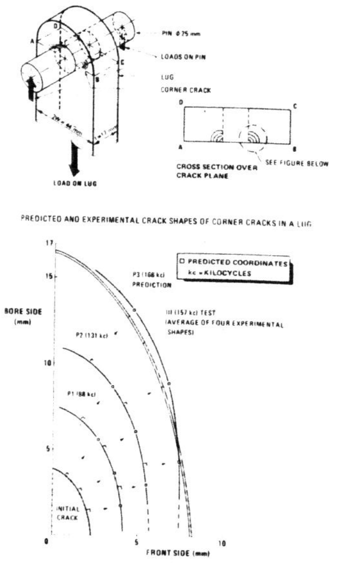

Fig. 33 A pin–loaded lug

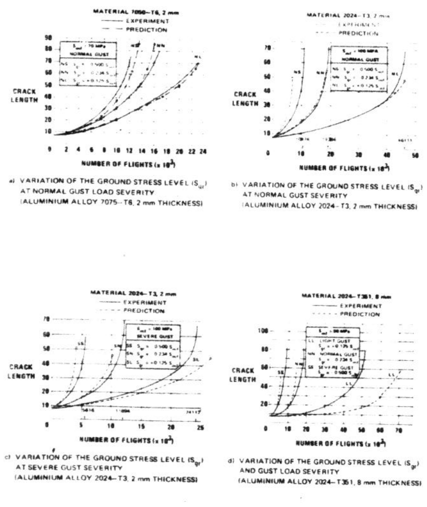

Fig. 32 Measured and predicted crack propagation curves

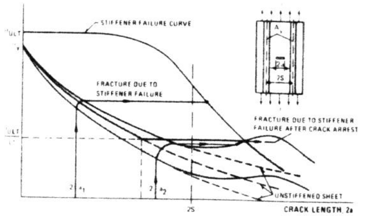

Fig. 34a Residual strength diagram for panel stiffened with light stringers

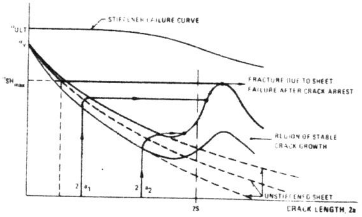

Fig. 34b Residual strength diagram for panel stiffened with heavy stringers

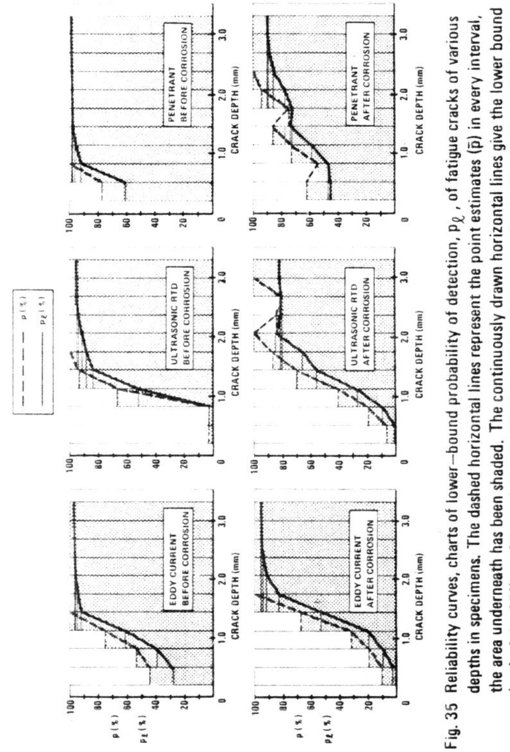

Fig. 35 Reliability curves, charts of lower–bound probability of detection, p_ℓ, of fatigue cracks of various depths in specimens. The dashed horizontal lines represent the point estimates ($\bar{p}$) in every interval, the area underneath has been shaded. The continuously drawn horizontal lines give the lower bound (p_ℓ) of the 95% confidence interval with the available data grouped according to the optimized probability method. To produce conservative graphs both types of calculated data were considered to be applicable to the largest flaw in each interval; therefore the right hand sides of the horizontal lines were connected.

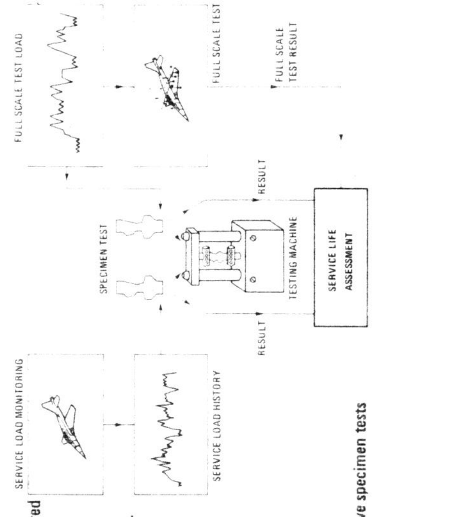

Fig. 36 Life re-assessment by comparative specimen tests

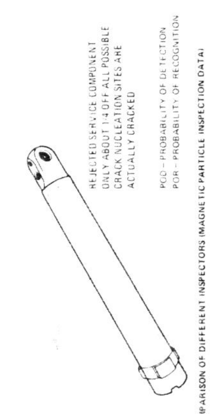

COMPARISON OF DIFFERENT INSPECTORS (MAGNETIC PARTICLE INSPECTION DATA)

INSPECTOR	MISSED FLAWS				SPURIOUS INDICATIONS			
	FLAWS NOT DETECTED	OUT OF FLAWED LUGS	PERCENTAGE MISSED	P.O.D ($p_{\ell\,95\%}$)	SPURIOUS INDICATIONS	OUT OF FLAW FREE LUGS	PERCENTAGE SPURIOUS	P.O.R ($r_{\ell\,95\%}$)
A	4	33	12.1	74.4	9	132	6.8	88.4
B	6	146	4.1	92.1	16	454	3.5	94.7
C	0	145	0.0	98.0	54	446	12.1	85.1
D	0	141	0.0	97.9	43	438	9.8	87.5

COMPARISON OF DIFFERENT METHODS

NUMBER OF INSPECTIONS INVOLVED	MISSED FLAWS				SPURIOUS INDICATIONS			
	FLAWS NOT DETECTED	OUT OF FLAWED LUGS	PERCENTAGE MISSED	P.O.D ($p_{\ell\,95\%}$)	SPURIOUS INDICATIONS	OUT OF FLAW FREE LUGS	PERCENTAGE SPURIOUS	P.O.R ($r_{\ell\,95\%}$)
3x US	198	330	60.0	35.5	17	1008	1.7	97.5
4x PT	72	334	21.6	74.4	65	1084	6.0	92.7
4x MPI	10	465	2.2	96.4	122	1470	8.3	90.4
4x MRI	29	344	8.4	88.7	48	1072	4.5	94.3
3x EC	53	288	18.4	77.4	115	894	12.9	85.1

Fig. 37 Evaluation of non-destructive inspection methods

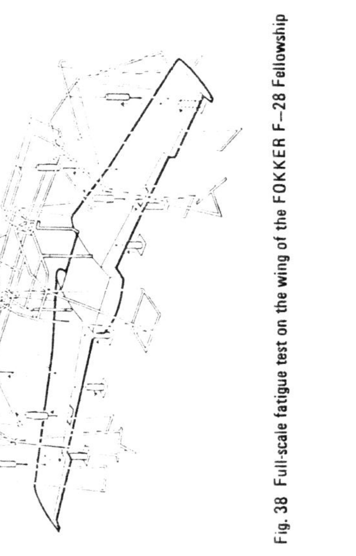

Fig. 38 Full-scale fatigue test on the wing of the FOKKER F–28 Fellowship